

Electronic Supplementary Information: Atomistic Insights into the Stabilization and Binding Mechanisms of MoS₂ Nanoflakes Supported on Graphene from an *ab initio* Investigation

Naidel A. M. S. Caturello,* Julian F. R. V. Silveira,* and Juarez L. F. Da Silva*

*São Carlos Institute of Chemistry, University of São Paulo, PO Box 780, 13560-970, São
Carlos, São Paulo, Brazil*

E-mail: naidel@usp.br; julian.vieira.silveira@gmail.com; juarez_dasilva@iqsc.usp.br

1 Introduction

The present electronic support information contains the following data:

1. Further details on the pre-optimizations performed with the ReaxFF calculations.
2. Convergence tests of the \mathbf{k} -points mesh and the comparison among the energies obtained using the Γ -point and the $2 \times 2 \times 1$ mesh.
3. All the final optimized (MoS₂)_n/Gr, $n = 4, 6, 9, 12, 16$ configurations along with their relative total energies, ΔE_{tot} .
4. (MoS₂)_n/Gr, $n = 4, 6, 9, 12, 16$ work functions for the most stable 2H-, 1T'-, stripe-, and 1D-MoS₂ nanoflakes.

5. Isosurfaces of the clean $(12 \times 6\sqrt{3})R60^\circ$ Gr relaxed supercell.
6. Further information into the HOMO, LUMO, and work functions values of gas-phase MoS₂ nanoflakes which compose the most stable (MoS₂)_n/Gr, $n = 1, 4, 6, 9, 12, 16$ and 2H-MoS₂/Gr bilayer isosurfaces and MoS₂/Gr.

2 Trial Configurations for the (MoS₂)_n Systems using Reactive Force Field as Implemented in LAMMPS

In order to reduce the computational demand of screening thousands of configurations to obtain a representative set, we established a procedure employing Reactive Force Field (ReaxFF) to optimize the initial set, which contained hundreds of thousands of configurations with different docking distances, angles and positions, and keep only the most significant configurations. The optimization procedure employed a conjugated gradient algorithm, with an energy tolerance criteria of 10^{-6} eV, and the lattice parameter was optimized in monolayers by allowing the simulations box to change during the optimization. The potential was employed as it accurately described the periodic monolayers of the materials, Figure S1.

Table S1: Comparison between structural properties obtained through DFT/PBE+TS^{1,2} calculations in the FHI-aims package,³ ReaxFF^{4,5} in the LAMMPS code,^{6,7} and experimental results.

Monolayer	Property	ReaxFF	DFT/PBE+TS	Experimental
2H-MoS ₂	a_0 (Å)	3.184	3.177	3.18 ⁸
1T'-MoS ₂	$d_{(100)}$ (Å)	5.582	5.702	5.72 ⁹
	$d_{(010)}$ (Å)	3.094	2.753	2.79 ⁹
Pristine-C ₂	a_0 (Å)	2.462	2.462	2.462 ¹⁰

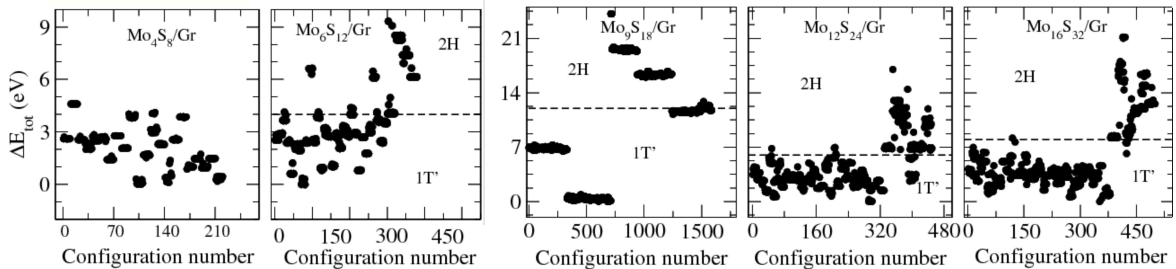


Figure S1: Energy distribution of the ReaxFF optimized $(\text{MoS}_2)_n/\text{Gr}$, $n = 4, 6, 9, 12$, num16 configurations used as pre-optimized structures for further DFT relaxation.

3 Computational DFT Convergence Tests

Since total energies differences are fundamental for our work, we performed \mathbf{k} -points mesh convergence in order to establish the most suitable grid to be used in our calculations. From Figure S2, we observed that the $2 \times 2 \times 1$ \mathbf{k} -points mesh is the smallest grid density allowing us to obtain energies in total energies consistent with more dense grids. Thus, we used this mesh for all the relaxation calculations performed within this this work. We also performed a comparison among the relative total energies of all the investigated $\text{Mo}_{16}\text{S}_{32}/\text{Gr}$ configurations using the $2 \times 2 \times 1$ \mathbf{k} -points mesh and solely the Γ -point, Table S2.

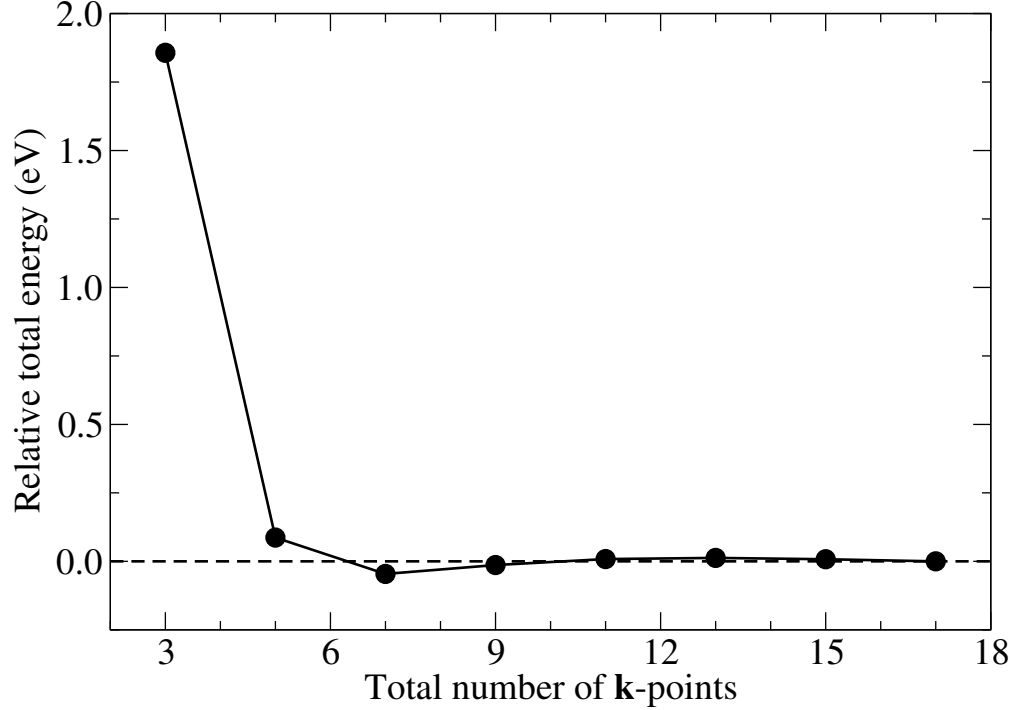


Figure S2: Convergence test for the 3×4 $\text{Mo}_{12}\text{S}_{24}$ on a $(6\times 3\sqrt{3})_{R-60^\circ}$ Gr monolayer as function of the total k-points. The k-points meshes used ranged from $1\times 1\times 1$ to $8\times 8\times 1$.

The differences in mesh grid densities provided dissimilar total energies in all systems. However, the relative total energies are in good agreement. This result suggests that large MoS_2 nanoflakes adsorbed in large Gr monolayers can be energetically evaluated using the Γ -point. However, since our intent herein is to evaluate structural and electronic properties, we employed a denser k-points mesh.

Table S2: Total energies, E_{tot} , and relative total energies, ΔE_{tot} , along with their respective names of the $\text{Mo}_{16}\text{S}_{32}$ nanoflakes adsorbed on the Gr sheets for calculations performed using the Γ point and $2\times 2\times 1$ the k -points mesh.

Mo ₁₆ S ₃₂ /Gr Configurations	Γ -point Calculations		$2\times 2\times 1$ k -mesh Calculations	
	E_{tot} (eV)	ΔE_{tot} (eV)	E_{tot} (eV)	ΔE_{tot} (eV)
2H (elongated)	-2426596.51317770	16.4802	-2426620.31525518	16.7075
2H (VS2; pseudo-4 \times 4)	-2426598.39630271	14.5971	-2426622.46119435	14.5616
2H (4 \times 4)	-2426599.12990317	13.8635	-2426622.90428496	14.1185
2H (vacancy; pseudo-4 \times 4)	-2426599.71200071	13.2814	-2426623.72298713	13.2998
2H (reconstructed triangle)	-2426605.31955451	7.6739	-2426629.44245283	7.5803
1D	-2426607.05635059	5.9371	-2426631.14663425	5.8762
2H (stripe)	-2426607.27752448	5.7159	-2426631.39191937	5.6309
1T' (unmatched trapeze)	-2426611.32312237	1.6703	-2426635.22318342	1.7996
1T' (elongated triangle)	-2426611.51188396	1.4815	-2426635.47899364	1.5438
1T' (elongated)	-2426611.61760539	1.3758	-2426635.54619756	1.4766
1T' (trapeze)	-2426611.77880465	1.2146	-2426635.66138268	1.3614
1T' (4 \times 4)	-2426612.99340730	0.0000	-2426637.02280037	0.0000

4 Optimized DFT-PBE+TS Configurations for $(\text{MoS}_2)_n/\text{Gr}$, where $n = 4, 6, 9, 12, 16$

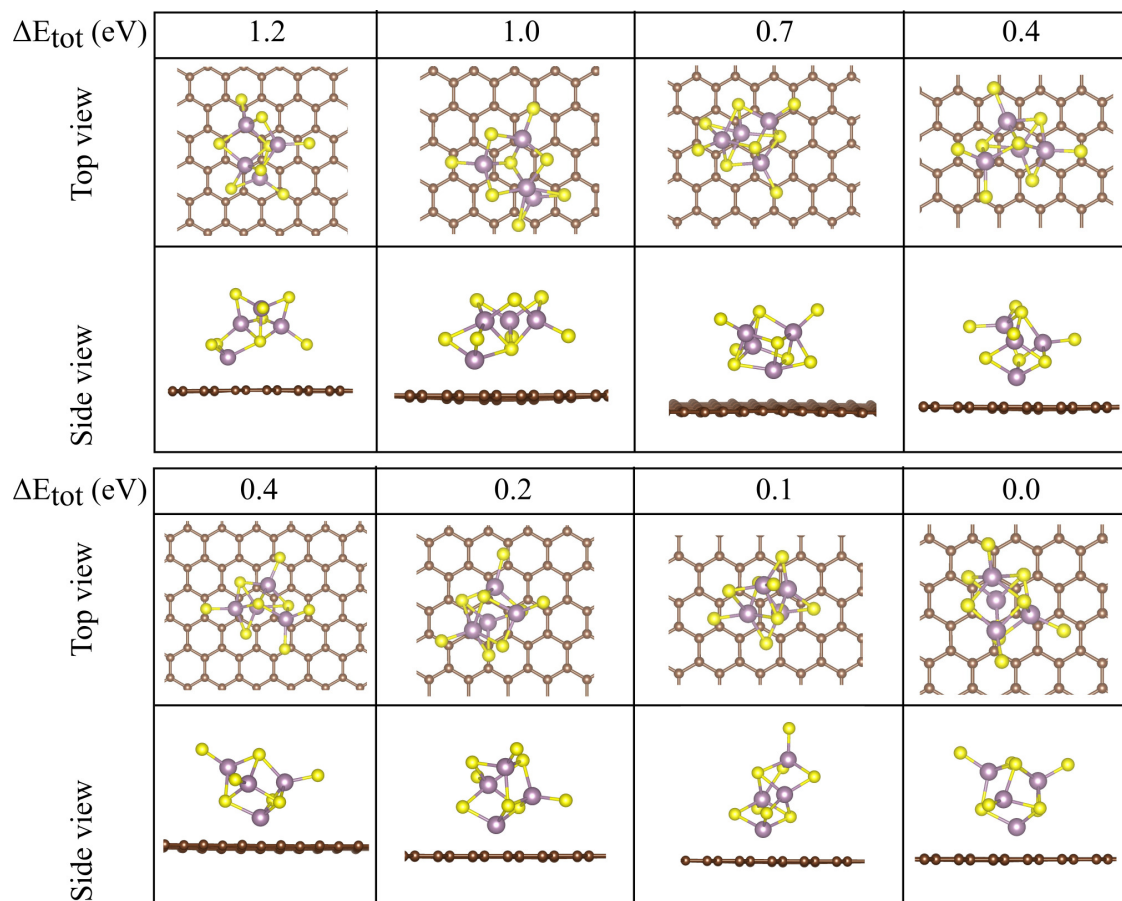


Figure S3: Top and side view of all DFT-optimized $\text{Mo}_4\text{S}_8/\text{Gr}$ configurations. The boxes defined the $(12 \times 6\sqrt{3})R60^\circ$ supercell used. The numbers over each configurations are the values of the total relative energies, ΔE_{tot} .

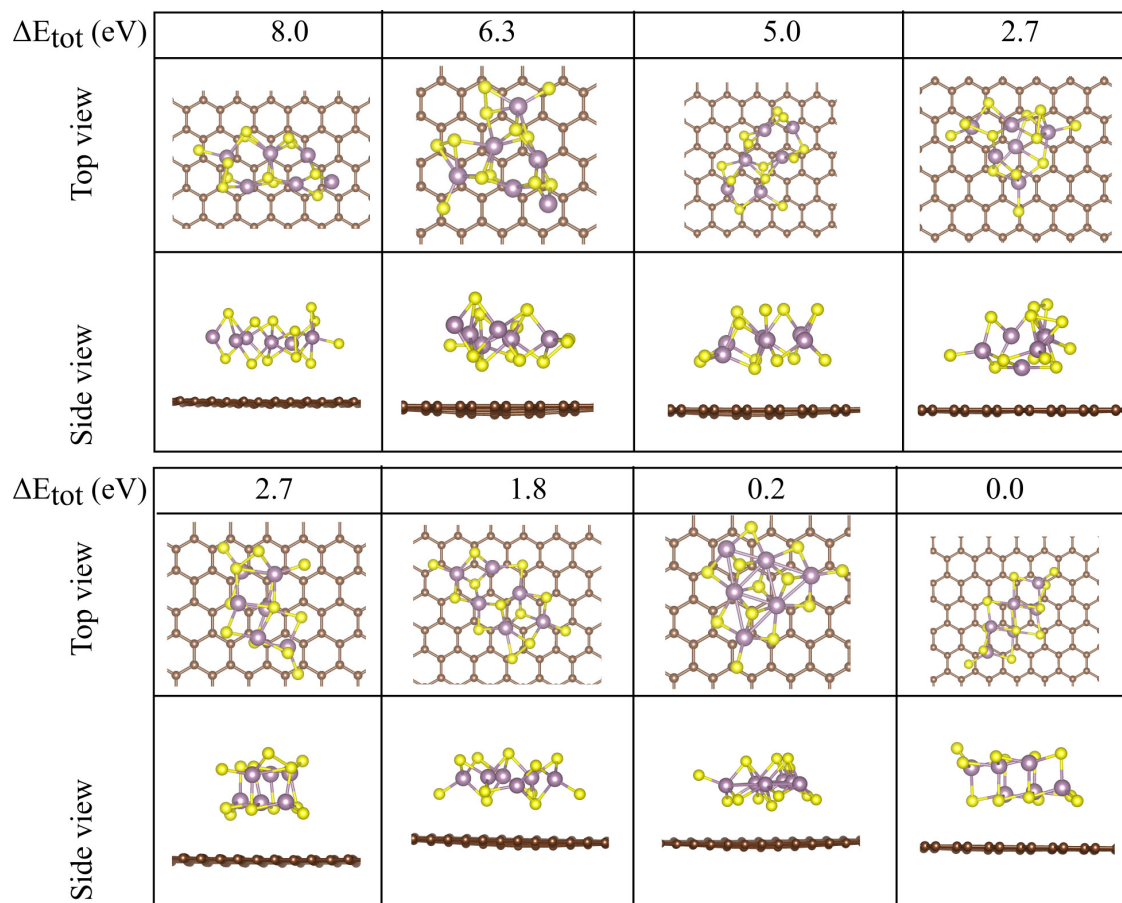


Figure S4: Top and side view of all DFT-optimized $\text{Mo}_6\text{S}_{12}/\text{Gr}$ configurations. The boxes defined the $(12 \times 6\sqrt{3})R60^\circ$ supercell used. The numbers over each configurations are the values of the total relative energies, ΔE_{tot} .

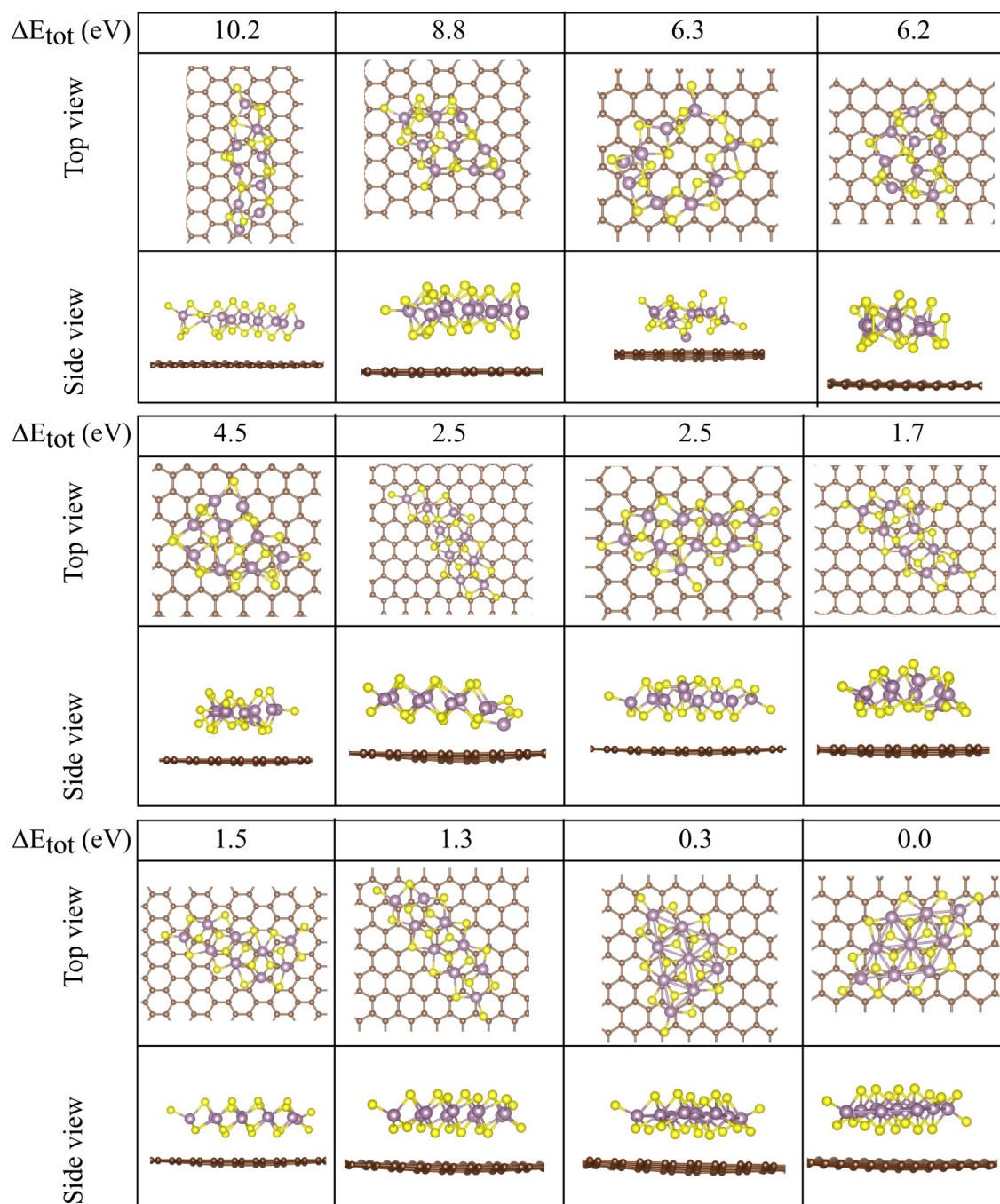


Figure S5: Top and side view of all DFT-optimized $\text{Mo}_9\text{S}_{18}/\text{Gr}$ configurations. The boxes defined the $(12 \times 6\sqrt{3})R60^\circ$ supercell used. The numbers over each configurations are the values of the total relative energies, ΔE_{tot} .

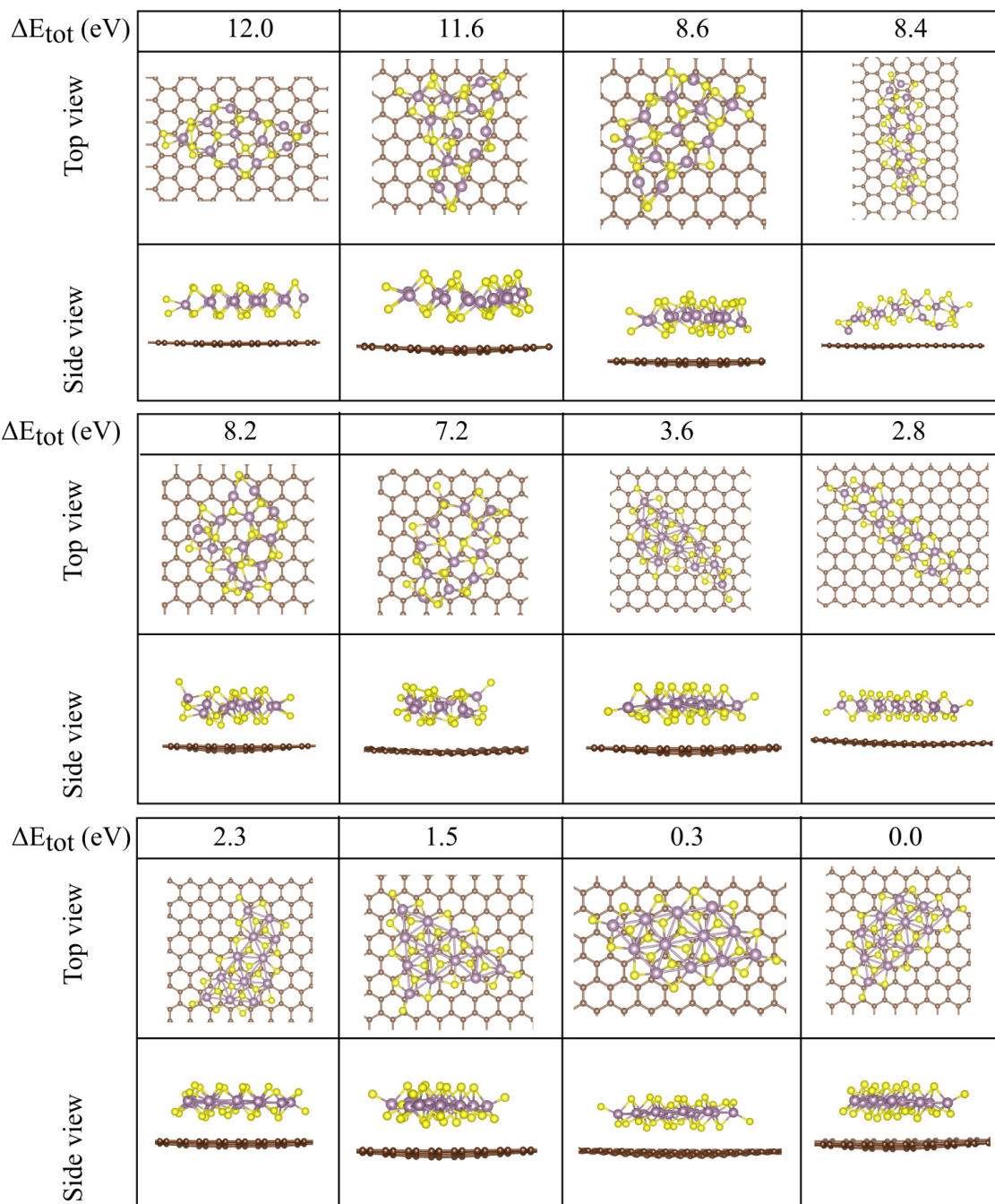


Figure S6: Top and side view of all DFT-optimized $\text{Mo}_{12}\text{S}_{24}/\text{Gr}$ configurations. The boxes defined the $(12 \times 6\sqrt{3})R60^\circ$ supercell used. The numbers over each configurations are the values of the total relative energies, ΔE_{tot} .

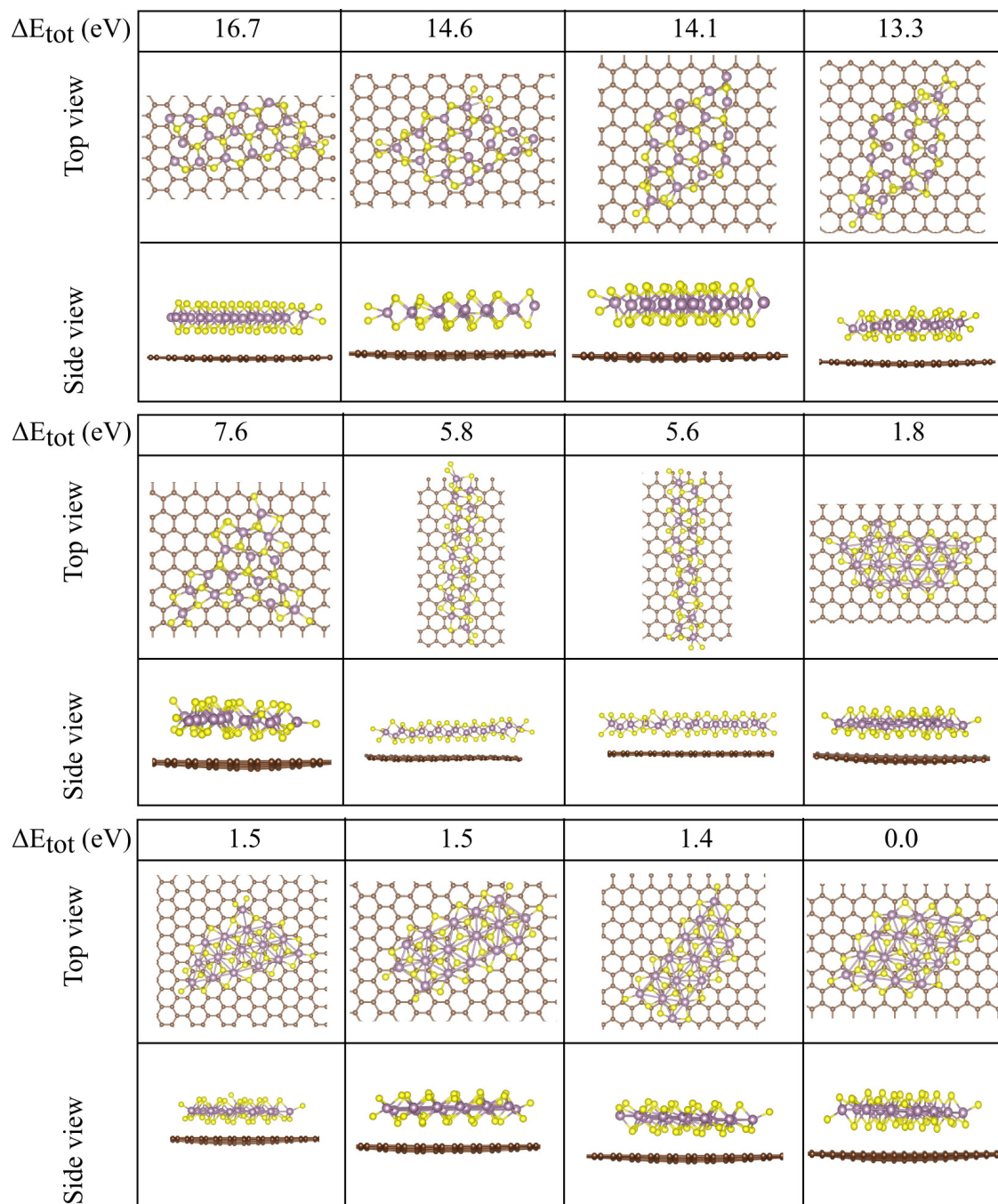


Figure S7: Top and side view of all DFT-optimized $\text{Mo}_{16}\text{S}_{32}/\text{Gr}$ configurations. The boxes defined the $(12 \times 6\sqrt{3})_{R-60^\circ}$ supercell used. The numbers over each configuration are the values of the total relative energies, ΔE_{tot} .

5 Density of States for the Ground-states Isomers

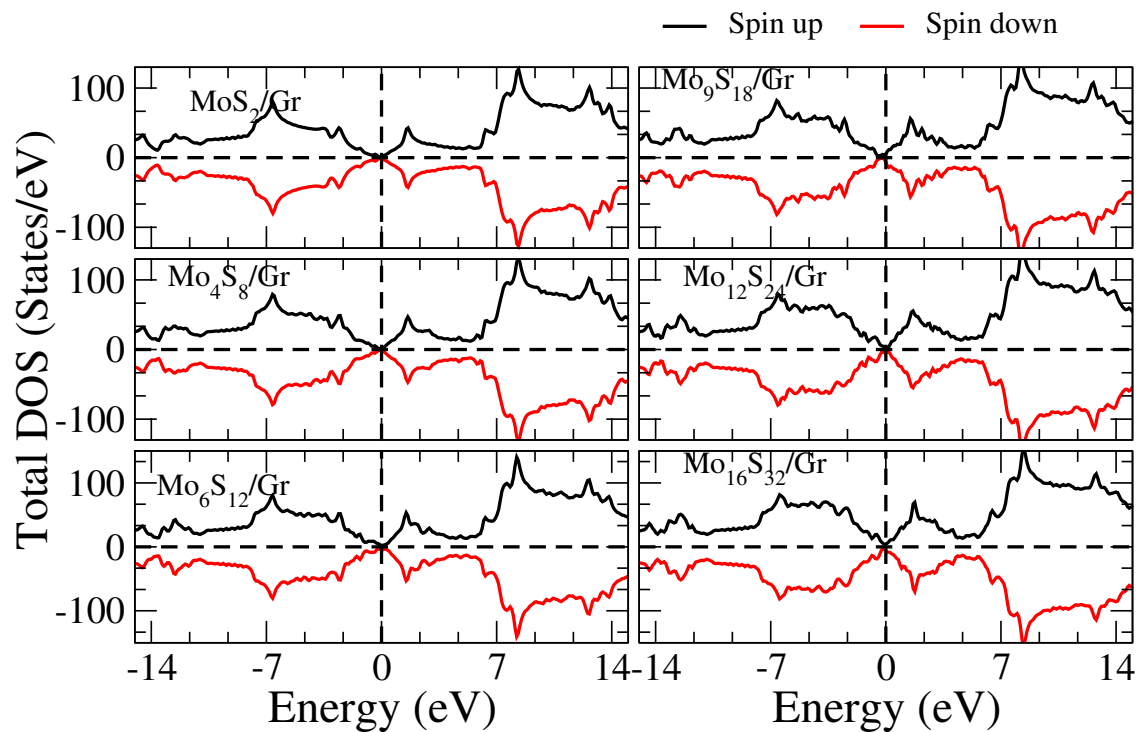


Figure S8: Total density of states of all $(\text{MoS}_2)_n/\text{Gr}$, $n = 1, 4, 6, 9, 12, 16$ ground-state configurations.

6 Work Functions for the MoS₂/Gr Systems

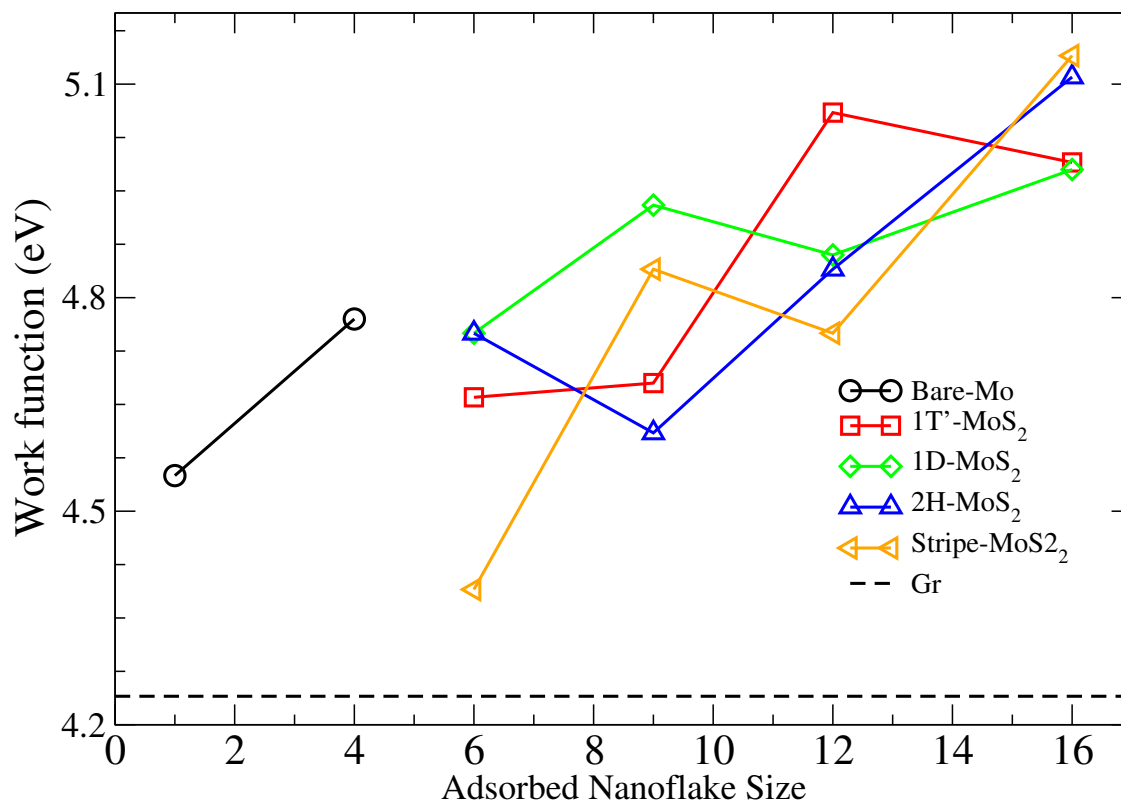


Figure S9: Work functions of the stacked MoS₂/Gr systems, with sorted by the adsorbed MoS₂ nanoflakes morphologies.

7 Clean Gr Supercell Isosurfaces

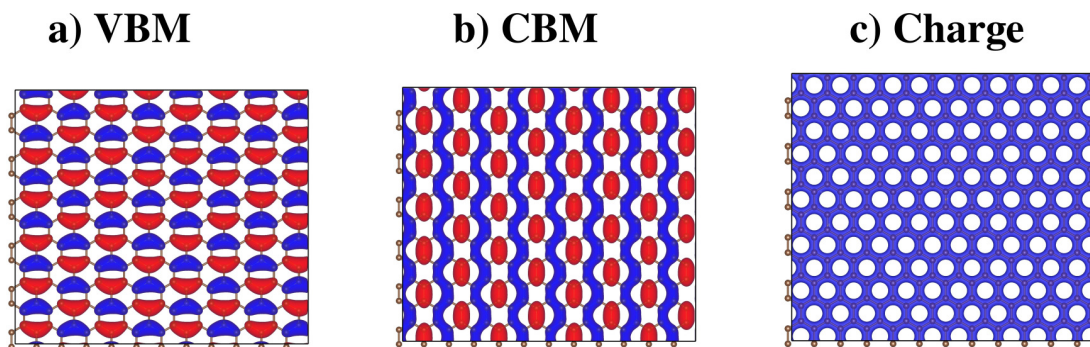


Figure S10: Orbital isosurfaces associated with the a) VBM and b) CBM of the $(12 \times 6\sqrt{3})R60^\circ$ Gr relaxed supercell; and c) the total charge, q , of the clean Gr supercell herein used.

8 Gas-Phase HOMO and LUMO values for MoS₂ Nanoflakes and 2H-MoS₂/Gr Bilayer VBM and CBM.

Table S3: Energy values of the HOMO and LUMO orbitals of the gas-phase (MoS₂)_n, $n = 1, 4, 6, 9, 12, 16$, along the values of VBM and CBM for the 2H-MoS₂ monolayers. All energies are in eV. The calculated work function of the 1T'-MoS₂ monolayer is 5.79 eV.

System	HOMO (VBM)	LUMO (CBM)	$\Delta E_{diff}^{\text{HOMO-LUMO}}$
MoS ₂	-5.12	-4.42	0.69
Mo ₄ S ₈	-5.65	-4.93	0.72
Mo ₆ S ₁₂	-5.62	-5.30	0.32
Mo ₉ S ₁₈	-5.69	-5.12	0.57
Mo ₁₂ S ₂₄	-5.66	-5.26	0.40
Mo ₁₆ S ₃₂	-5.58	-5.33	0.26
2H-MoS ₂	-5.85	-4.40	1.44

References

- (1) Tkatchenko, A.; Scheffler, M. Accurate Molecular van Der Waals Interactions from Ground-State Electron Density and Free-Atom Reference Data. *Phys. Rev. Lett.* **2009**, *102*, 073005.
- (2) Tkatchenko, A.; DiStasio, R. A.; Car, R.; Scheffler, M. Accurate and Efficient Method for Many-Body van der Waals Interactions. *Phys. Rev. Lett.* **2012**, *108*, 236402.
- (3) Blum, V.; Gehrke, R.; Hanke, F.; Havu, P.; Havu, V.; Ren, X.; Reuter, K.; Scheffler, M. Ab Initio Molecular Simulations With Numeric Atom-Centered Orbitals. *Comp. Phys. Comm.* **2009**, *180*, 2175–2196.
- (4) van Duin, A. C. T.; Dasgupta, S.; Lorant, F.; Goddard, W. A. ReaxFF: A Reactive Force Field for Hydrocarbons. *J. Phys. Chem. A* **2001**, *105*, 9396–9409.
- (5) van Duin, A. C. T.; Strachan, A.; Stewman, S.; Zhang, Q.; Xu, X.; Goddard, W. A.

- ReaxFFSiOReactive Force Field for Silicon and Silicon Oxide Systems. *J. Phys. Chem. A* **2003**, *107*, 3803–3811.
- (6) Plimpton, S. Fast Parallel Algorithms for Short-Range Molecular Dynamics. *J. Comput. Phys.* **1995**, *117*, 1–19.
- (7) Aktulga, H.; Fogarty, J.; Pandit, S.; Grama, A. Parallel reactive molecular dynamics: Numerical methods and algorithmic techniques. *Parallel Comput.* **2012**, *38*, 245–259.
- (8) Steinhoff, A.; Kim, J.-H.; Jahnke, F.; Rösner, M.; Kim, D.-S.; Lee, C.; Han, G. H.; Jeong, M. S.; Wehling, T. O.; Gies, C. Efficient Excitonic Photoluminescence in Direct and Indirect Band Gap Monolayer MoS₂. *Nano Lett.* **2015**, *15*, 6841–6847.
- (9) Yu, Y. et al. High Phase-Purity 1T'-MoS₂- and 1T'-MoSe₂-Layered Crystals. *Nat. Chem.* **2018**, *10*, 638–643.
- (10) Zhao, Y. X.; Spain, I. L. X-Ray Diffraction Data for Graphite to 20 GPa. *Phys. Rev. B* **1989**, *40*, 993–997.